Ultrasonics Sonochemistry 89 (2022) 106159

Contents lists available at ScienceDirect

Ultrasonics Sonochemistry

journal homepage: www.elsevier.com/locate/ultson

Characterization of cavitation under ultrasonic horn tip – Proposition of an acoustic cavitation parameter

Gregor Kozmus, Jure Zevnik, Marko Hočevar, Matevž Dular, Martin Petkovšek *

University of Ljubljana, Faculty of Mechanical Engineering, Aškerčeva 6, 1000 Ljubljana, Slovenia

ARTICLE INFO

Keywords:
Acoustic cavitation
Cavitation number
Ultrasonic horn
Salt solutions

ABSTRACT

Acoustic cavitation, generated by a piezo-driven transducer, is a commonly used technique in a variety of processes, from homogenization, emulsification, and intensification of chemical reactions to surface cleaning and wastewater treatment. An ultrasonic horn, the most commonly used acoustic cavitation device, creates unique cavitation conditions under the horn tip that depend on various parameters such as the tip diameter, the driving frequency of the horn, its amplitude, and fluid properties. Unlike for hydrodynamic cavitation, the scaling laws for acoustic cavitation are poorly understood. Empirical relationships between cavitation dynamics, ultrasonic horn operating conditions, and fluid properties were found through systematic characterization of cavitation under the tip. Experiments were conducted in distilled water with various sodium chloride salt concentrations under different horn amplitudes, tip geometries, and ambient pressures. Cavitation characteristics were monitored by high-speed (200,000 fps) imaging, and numerous relations were found between operating conditions and cavitation dynamics. The compared results are discussed along with a proposal of a novel acoustic cavitation parameter and its relationship to the size of the cavitation cloud under the horn tip. Similar to the classical hydrodynamic cavitation number, the authors propose for the first time an acoustic cavitation parameter based on experimental results.

1. Introduction

Cavitation is described as an instability within the liquid, caused by a local pressure drop. In the case of acoustic cavitation, acoustic waves result in pressure oscillations, causing liquid to break at the position of the nuclei when the pressure drops below the critical pressure. Small bubbles are formed that repeatedly grow and collapse. On the other hand, hydrodynamic cavitation is caused by a local pressure drop due to the interaction between the liquid and the wetted surfaces. In this case, the bubbles reach only one or a few rebounds before being carried away by the main flow.

The effects of acoustic cavitation were already studied almost a hundred years ago [1]. Since then, thousands of papers regarding this topic have been published. Nowadays, acoustic cavitation is mainly used within chemical and biological laboratory environments for various processes such as emulsification [2,3], homogenization or other process intensifications [4]. The most commonly used device is an ultrasonic horn, which is driven by a piezo transducer. Oscillations generated by a piezoelectric element are transmitted through a stepped or tapered extension, where amplified tip movements cause acoustic waves. Tip geometries can vary from flat [5], half-spherical [6] or conical shapes [7], yielding different patterns of acoustic flows. Periodically induced acoustic oscillations cause cavitation bubbles to form and collapse in a violent manner. Conditions under the horn tip can be varied by oscillating frequency, displacement amplitude and size of the tip. A large number of cavitation bubbles of various sizes are generated due to intense pressure waves induced by moving solid body through the liquid. Their structural formations resembles various shapes and were labelled such as streamers, clusters [8], cone like shapes [9] and even mushroom like shape – the acoustic supercavitation [10]. In addition, the occurrence and dynamics of cavitation can be strongly influenced by the physical properties of the liquid. The higher the vapor pressure for example, the higher is the probability of cavitation development at given conditions. A lower surface tension initially accelerates growth of the bubble, but then slows down its collapse [11]. On the other hand, viscosity does not play an important role at low values but can completely change the cavitation dynamics in highly viscous liquids [12]. The number, size distribution, and interactions of gas nuclei can be

* Corresponding author.
E-mail address: martin.petkovsek@fs.uni-lj.si (M. Petkovšek).

https://doi.org/10.1016/j.ultsonch.2022.106159
Received 6 May 2022; Received in revised form 24 August 2022; Accepted 2 September 2022
Available online 6 September 2022

significantly altered by addition of ionic salts. They adsorb on bubble–liquid interface and change the surface tension, surface charge, and the magnitude of intermolecular forces within the liquid film, formed between the bubbles. Therefore, the bubble interactions are affected, normally resulting in coalescence inhibition. This phenomenon was studied by several authors, revealing its highly non-linear dependency on salt concentration [13–15]. They found out that the coalescence is considerably inhibited only above particular salt concentration, called the transition concentration, which depends on the chemical structure of the salt. Recently, some authors reported that the bubble approach velocity is also an important factor in coalescence occurrence [16–18]. Various authors already studied the acoustic cavitation in salt solutions. They reported several differences in cavitation appearance, dynamics, and effects in comparison to the cavitation in pure water [19–21]. In general, increasing salt concentration leads to a larger bubble population, with smaller and more stable bubbles. Furthermore, the addition of salts can also affect the average distance between neighbouring bubbles – bubble cloud density [22]. Its response to an ultrasonic wave can be altered consequently.

Due to the complexity of the phenomena, it is difficult to objectively compare the extent and dynamics of acoustic cavitation under different process parameters, such as different liquid properties or characteristics of the ultrasonic device. Therefore, the experimental results from different authors are difficult or even impossible to compare, which slows down the progress in the research of cavitation exploitation in various processes. Furthermore, forecasting the results of ultrasonic sample processing can be inaccurate and is mostly experience based. For comparison between experiments, a dimensionless parameter called cavitation number is often used in hydrodynamic cavitation research. Its definition can take a variety of similar forms, but is usually expressed by the following equation:

$$\sigma = \frac{p_\infty - p_v(T)}{\frac{1}{2}\rho v^2}, \tag{1}$$

where p_∞ is pressure at some reference point, p_v is liquid vapour pressure at bulk liquid temperature T, ρ is liquid density, and v is flow velocity at location of interest [11]. While some attempts have been recently made to obtain a similar parameter for acoustic cavitation [23], it still lacks a broader empirical validation.

Although commonly used in hydrodynamics, the cavitation number is often overused and inadequately extrapolated, as shown by Šarc et al. [24]. The specified form of hydrodynamic cavitation number (Eq. (1)) does not take into account the effects of channel geometry, liquid viscosity and surface tension, amount of dissolved gasses, thermal effects due to liquid temperature, and many others. Some of these variables were considered by Keller [25], who managed to empirically correlate cavitation inception with some hydrodynamic parameters and obtain a scaling relation. However, these parameters can significantly affect the extent of cavitation, its dynamics, and its effects. Similarly, acoustic cavitation generated by an ultrasonic homogenizer is characterized by device properties (operating frequency, amplitude, horn geometry, and tip diameter), liquid properties (vapour pressure, temperature, viscosity, surface tension, speed of sound, dissolved gas content), and experimental parameters (ambient pressure, horn immersion, operating power, proximity of vessel walls, etc.). These parameters can have a significant impact on homogenizer performance. Ideally, they would all be accounted for in some form of dimensionless parameter or model. However, few authors have attempted to make progress in this area [26,27].

To characterize and model the effects of the physical properties of the liquid on the cavitation size and dynamics of cavitation, one must alter physical properties in a controlled manner. This can be done by adding different amounts of salt, for example sodium chloride (NaCl). High purity NaCl is low-cost and there is a large amount of data on the properties of NaCl-water solutions (surface tension, viscosity, vapor pressure, speed of sound, etc.) at different concentrations. In addition, most properties are linearly dependent on NaCl concentration. Sodium chloride solutions are also widely used in chemistry, microbiology, and material science, with many applications involving ultrasonic cavitation [28–30].

2. Materials and methods

Cavitation phenomena were studied using a Cole-Palmer 750 W ultrasonic homogenizer (UH) with driving frequency of 20 kHz and two tip diameters (3 and 4.8 mm) in various water solutions (Table 1). UH was installed in a closed stainless steel vessel that provided the ability to control ambient pressure and liquid temperature. The vessel (Fig. 1) had four tempered glass observation windows on each side and an additional observation window on the bottom. The top of the vessel served as a lid with connections for the pressure transducer, the power supply for the sonotrode, and the opening for sample insertion. At the bottom of the vessel a valve for the sample release was installed and a Pt100 probe to monitor the temperature of the liquid, which was maintained at 25° C ± 0.5° C. The pressure inside the vessel was regulated by a laboratory compressed air system and monitored by an absolute pressure transducer ABB 266AST with a measuring range between 0 and 10 bar. The ultrasonic horn could be moved vertically so that the immersion depth of the horn and the distance of the horn from the bottom of the vessel could be precisely adjusted. The distance to the bottom was kept constant at 5 cm, whereas the immersion depth was 4 cm for main part of the study but also finely swept from 0 to 9 cm at specific operating conditions.

The main part of cavitation analysis included four different solutions, all based on distilled water with different amounts of added sodium chloride salt (NaCl): pure distilled water (DW), saline solution (FW) with 9 g of salt per 1 kg of water (9 ‰ salinity), standard seawater (SW) with 35 ‰ salinity, and approximately saturated solution (SAT) with 360 ‰ salinity. Experiments within listed solution were performed by UH with tip diameters 3 and 4.8 mm, at different ambient pressures (p_∞) of 100, 200 and 300 kPa and three different settings of the horn amplitude: 20 %, 30 %, and 40 % of the maximum amplitude. Additionally, the salinity was finely swept from 0 to 36 % at constant ambient pressure (100 kPa), amplitude setting (40 %) and tip diameter (3 mm). The ambient pressure was also gradually varied from 75 to 300 kPa absolute pressure in DW, with 3 mm tip and 40 % amplitude setting.

A laboratory precision balance (±0.01 g) was used to weigh the required amount of salt, which was then dissolved in water using a magnetic stirrer. The density of the samples was measured using a measuring cylinder and a precision balance. Other properties of the water and salt solution (viscosity, surface tension, vapor pressure, and speed of sound) were obtained from the literature. All properties of the samples are summarised in Table S1.

The corresponding amplitudes, expressed in micrometres, were determined by analysing the movement of the horn in the air (the results are given in Supplementary Material, Table S2). Since the power consumption of the horn depends on the density and viscosity of the liquid, we measured the power absorbed by the ultrasonic device online during all experiments using the Fluke Norma 4000 power analyser. It was then

Table 1
Results of nonlinear regression analysis.

Exponent (Variable)	Optimal value	95 % confidence interval		p – value	Selected value
A (Δp)	− 1.10	−1.20	−1.01	2×10^{-39}	−1
B (P)	1.19	1.05	1.33	3×10^{-30}	1
C (d)	1.00	0.84	1.17	6×10^{-21}	1
D (c)	− 0.66	−1.02	−0.30	4×10^{-4}	−1
E (h)	−0.14	−0.24	−0.05	0.004	0

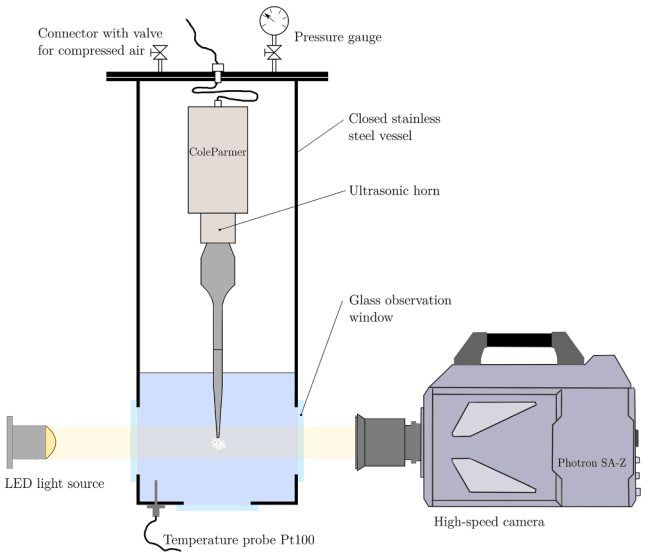

Fig. 1. Experimental set-up.

averaged over a 5-second interval to obtain the mean power of the device.

Cavitation characterization was performed using the high-speed visualisation method. Visualisation was performed using the Photron Fastcam SA -Z high-speed camera (CMOS sensor), with a frame rate of 200,000 fps at a resolution of 256 × 224 pixels. The exposure time was set to 10 μs. The illumination was set from the back and provided sharp and high-contrast images (Fig. 2). High power LEDs were used to enable short shutter time and a relatively closed aperture on the 105 mm Nikkor lens. The raw images were post – processed to evaluate the size of the cavitation cloud on each image. Data from a sequence of 20 000 images was then averaged to obtain the mean cavitation cloud size value for a given set of experimental conditions. Afterwards, a Fast Fourier Transform (FFT) of the cavitation cloud size temporal function was used to calculate frequency spectra and characteristic frequency peaks of cavitation cloud size oscillations.

3. Results and discussion

Characterization of cavitation in distilled water and various NaCl solutions is presented using high-speed visualizations. Comparison in different solutions under selected operating conditions and different tip diameters is discussed in terms of cavitation size and cavitation dynamics. The cavitation size is represented by the area of the cavitation cloud projection (black structures in Fig. 2) due to the simplicity and straightforwardness of the method. Cavitation dynamics is represented by characteristic frequencies of cavitation cloud oscillations determined by FFT analysis of temporal changes in cavitation cloud size.

3.1. Pressure dependency

Fig. 2 presents a typical evolution of cavitation under an UH tip in distilled water for three different static ambient pressures: 100 kPa, 200 kPa, and 300 kPa. The cases shown were performed at 40 % of the UH amplitude setting, corresponding to a peak amplitude of 270 μm. The image sequences shown have the same time step of $\Delta t = 0.05$ ms and the individual images follow from left to right. In all three cases, the first image shows the moment when cavitation cloud collapses, which corresponds to the stage of minimum cloud size. In the following images, at least one cycle of cavitation growth and collapse can be seen. At an ambient pressure of 100 kPa, one cycle is seen, at 200 kPa one and a half, while at 300 kPa two growth-collapse cavitation cycles can be determined. The size comparison confirms that the overall extent of cavitation decreases with increasing ambient pressure. On the other hand, increasing ambient pressure leads to a higher frequency of the growth-collapse cavitation cycle. Cavitation size is reduced in the radial and axial directions with increasing pressure. While at 100 kPa a fully formed cavitation structure under the UH tip resembles mushroom shape (4th and 5th image), with increasing pressure the cavitation shape loses mushroom shape and settles at the UH tip. One can also distinguish between the main cavitation structure under the UH tip (black, uniform shape) and the cavitation background in the near region below the main cavitation structure. A closer look reveals that the background cavitation becomes denser as the ambient pressure increases. The liquid becomes more opaque as the number of individual cavitation bubbles increases, which become smaller at higher ambient pressure.

The left side of Fig. 3 presents average cavitation cloud size and typical cavitation cloud oscillation frequencies for the UH tip with a diameter of 4.8 mm in distilled water under various ambient pressures and horn amplitudes. The filled grey bars show the average cavitation size, while the striped bars represent the typical frequencies of the cavitation cloud size oscillations. The values shown for the cavitation size are the average values of the cloud projection area in mm^2 and are considered as the size parameters of the cavitation structure. The frequency determination is based on FFT calculations of the temporal cavitation size and finding frequency peaks in the frequency spectra (the right side of Fig. 3 shows the frequency spectra for UH amplitude setting of 40 % in DW under different ambient pressures).

As already observed in Fig. 2, diagram on the left side of Fig. 3 clearly shows that the size of cavitation decreases with increasing ambient pressure. The decreasing trend can be seen for all three horn amplitude settings 20 %, 30 %, and 40 %, respectively. As expected, the cavitation size increases with increasing horn amplitude at all three ambient pressures. However, the size of the cavitation cloud decreases rapidly with increasing ambient pressure at an amplitude setting of 40 %. On the other hand, this decrease is smaller at an amplitude setting of 30 % and minimal at 20 % (Fig. 3, filled bars). This trend is additionally illustrated by dotted lines. It seems that with increasing ambient pressure, the cavitation growth at increasing amplitude is declined. This could be due to amplified energy dissipation through the wetted part of the horn tip.

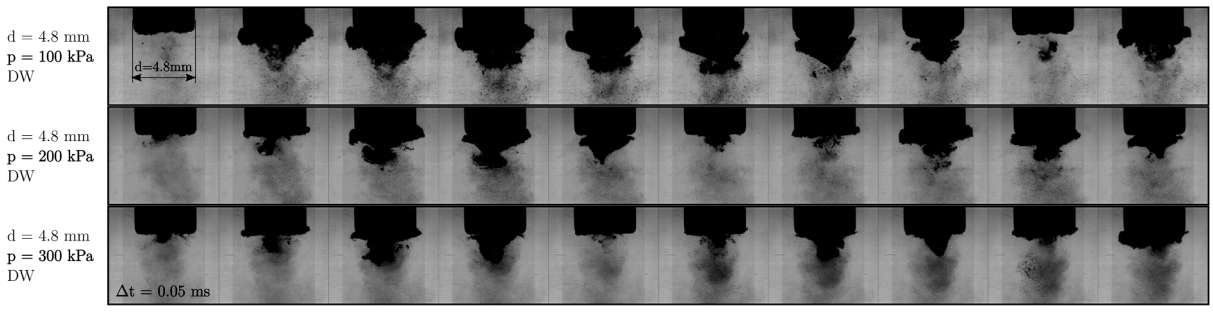

Fig. 2. Typical cavitation structure formation under UH tip d = 4.8 mm in distilled water at three different ambient pressures 100, 200, and 300 kPa at 40 % UH amplitude setting (actual amplitude = 270 μm). The time step between consecutive images (0.05 ms) matches the time step of one acoustic cycle of UH.

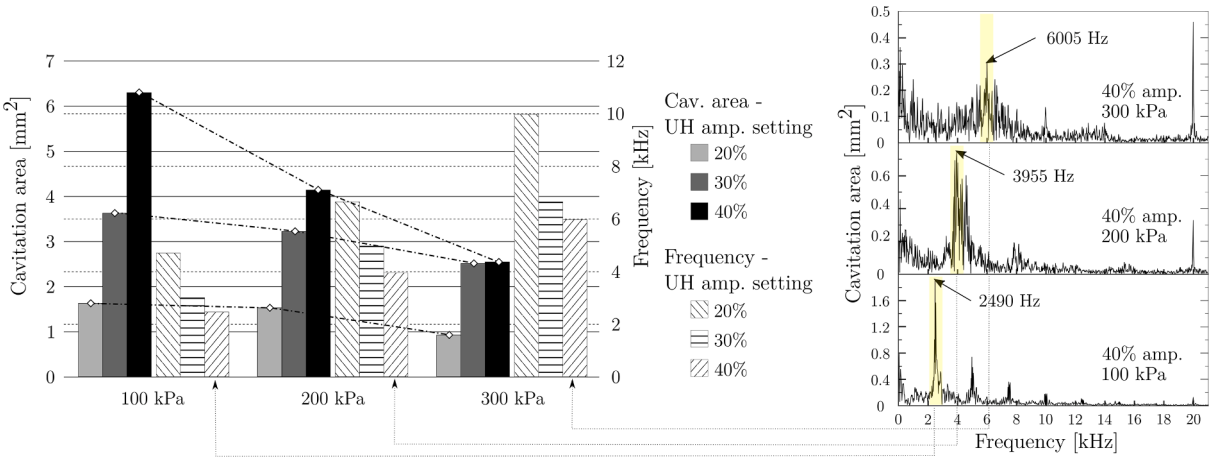

Fig. 3. Left: Average cavitation cloud size (filled bars) and characteristic frequencies of cloud oscillations (stripped bars) under UH tip with 4.8 mm diameter, operating in DW at various ambient pressures and amplitude settings. Filled bars with the same amplitude setting are connected with dotted lines, representing distinct trends of increasing ambient pressure effects. Right: Frequency spectra of cavitation cloud area oscillation under the same 4.8 mm tip in DW. Only cases at 40 % amplitude setting and at 100, 200, and 300 kPa ambient pressure are shown. Characteristic frequency peaks are highlighted.

When the ambient pressure is increased, the size of the cavitation cloud is suppressed, and part of the horn tip comes into direct contact with the liquid (Fig. 2, 200 kPa and 300 kPa). Part of the acoustic energy is therefore dissipated directly into the liquid phase, which has a much higher acoustic impedance compared to the vaporous cavitation cloud. This leads to additional energy consumption at high ambient pressures, and the development of the cavitation cloud is consequently hindered. A similar spatial contraction of the cavitation cloud was observed by Tzanakis et al. [6] in a highly viscous liquid.

To compare the main cavitation frequencies, the most powerful peaks in the frequency spectra were determined (Fig. 3 - right) and plotted in the dashed bars (Fig. 3 - left) for better comparison. Despite the constant driving frequency of the horn (20 kHz), cavitation under the tip is still a chaotic phenomenon, so isolated peaks are not always seen in the frequency spectrum. The main cavitation cloud oscillation frequency generally increases with increasing ambient pressure, while it decreases with increasing horn amplitude. The cavitation cloud dynamics is closely related to the cavitation cloud size, the two being inversely correlated. As the cavitation size increases, the main cavitation frequency decreases because the cavitation takes more time to grow and consequently the collapse takes longer. A comparison of the maximum – 6.3 mm^2 (pressure 100 kPa at 40 % amplitude) and minimum – 0.9 mm^2 (pressure 300 kPa and 20 % amplitude) average cavity size under the horn tip shows that the oscillation frequency is lowest at maximum cavity size – 2490 Hz, while the oscillation frequency is highest in case of minimum cavity size – 10000 Hz. When one increases the ambient pressure, the typical cloud oscillation frequency becomes not only higher, but also much less pronounced. At 100 kPa ambient pressure, an isolated frequency peak with three distinct higher harmonics can be observed (Fig. 3 - right). On the other hand, the frequency spectrum is more scattered at 300 kPa. Smaller cavitation clouds at high ambient pressures have a characteristic oscillation frequency that appears to be out of phase with the horn motion, resulting in chaotic behaviour under the tip, which further hinders the cloud's evolution. Occasionally, the nominal frequency of the horn is forcibly introduced into the dynamics of the cavitation cloud, resulting in a pronounced peak at 20 kHz (cases at 200 kPa and 300 kPa ambient pressure in Fig. 3 - right). The peak at 20 kHz is less pronounced at 100 kPa due to the higher inertia of the relatively large cavitation cloud, which is less sensitive to external disturbances. Comparing the frequency spectra with those obtained by Yusuf et al. [27] in a similar study, one can notice interesting dissimilarities. In our case, the fundamental peaks of UH are much less pronounced, while Yusuf et al. obtained very pronounced fundamental peaks under all operating conditions. However, they calculated the frequency spectra from the acoustic emission measured by a pressure sensor. It is expected that a sonotrode will always emit a high amplitude pressure wave at its fundamental frequency, even the cavitation cloud does not collapse at that moment. On the other hand, only cavitation cloud oscillations are detected by the imaging technique used in our study. Nevertheless, it would be interesting to couple the frequency analysis of cavitation cloud size oscillations and acoustic emissions in future studies.

To further study the relationships between ambient pressure, cavitation size and UH power consumption, the ambient pressure was varied gradually from 75 to 300 kPa by 25 kPa increments. Experiments were performed in DW only, with 3 mm tip at 40 % amplitude setting. Results are presented in Fig. S2 in Supplementary material. It can be confirmed that the cavitation cloud size continuously decreases with increasing ambient pressure. On the other hand, the power consumption steadily increases as ambient pressure is increased.

3.2. *Dependence on liquid properties*

By adding sodium chloride (NaCl) salt to the water matrix, the physical properties of the solutions, such as viscosity, surface tension, vapor pressure, and speed of sound can be modified in a controlled manner (Table S1). Furthermore, these properties are linearly dependent on NaCl concentration. In this section, we present a comparison of cavitation in distilled water (DW) with cavitation in three different NaCl solutions with 9 ‰, 35 ‰, and 360 ‰ salinity (grams of salt per kg of water). The 9 ‰ solution mimics a concentration commonly used in biology and medicine, the 35 ‰ solution corresponds to the salinity of standard seawater, and the 360 ‰ is a saturated solution at 25 °C. A comparison of cavitation appearance under UH tip of 4.8 mm diameter at 200 kPa ambient pressure and 40 % horn amplitude setting is presented in Fig. 4. The first image sequence shows cavitation in distilled water. The lower image sequences show NaCl solutions with 9 ‰, 35 ‰, and 360 ‰ salinity, respectively. The time step between each image in each sequence is constant and equals 0.05 ms. It can be seen that the size of the cavitation cloud (the coherent gaseous-vapor phase structure) surges with increasing salinity up to 35 ‰, but then contracts at 360 ‰ salinity. This trend is even more evident when considering the background cavitation (a dimmed region below the cavitation cloud). The latter is a consequence of the microbubble clusters being present in the solution, which act as cavitation nuclei when shock waves pass through the liquid. When the salinity is increased to 35 ‰, these clusters appear larger and denser, but apparently disappear completely at 360 ‰. However, when a shock wave passes through the solution, their presence

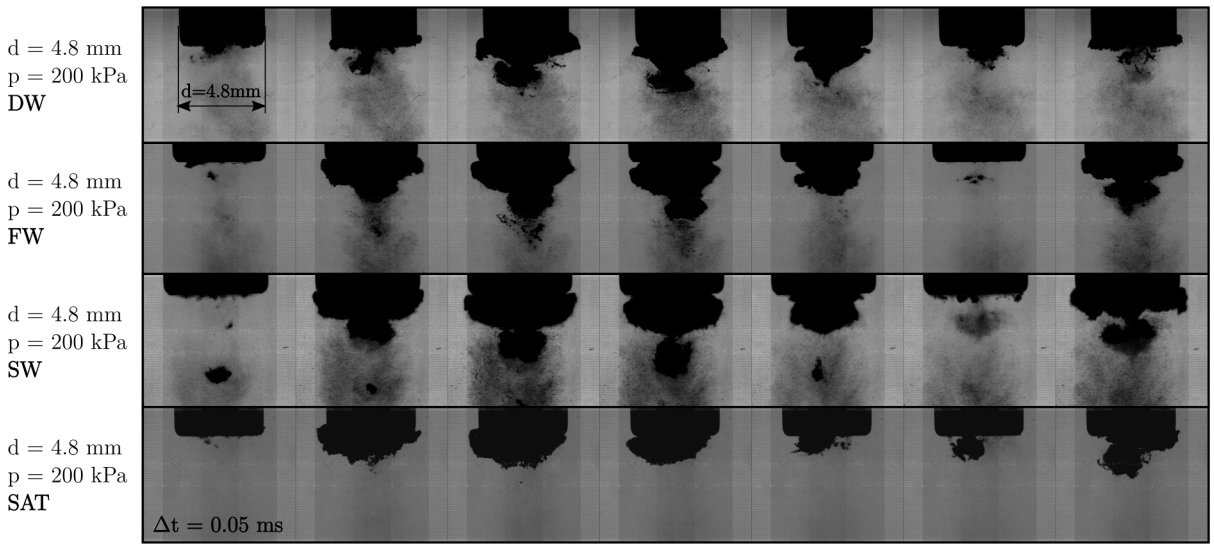

Fig. 4. Typical cavitation cloud formation under UH tip d = 4.8 mm in various saline solutions at operating conditions 200 kPa and 40 % amplitude.

can be clearly observed (Video1, Supplementary Material). The differences in the number and size of cavitation nuclei at different salt concentrations can be explained by the phenomenon of coalescence inhibition. When salts are added to the water matrix, they adsorb on bubble - liquid interface and prevent the drainage of the liquid film between two bubbles upon contact, thus inhibiting their coalescence [31]. This results in higher number and smaller size of microbubbles present in the solution. The surface tension, which increases with increasing salinity, shrinks the bubbles further and stabilizes them at a smaller average diameter.

The left part of Fig. 5 shows the average cavitation size (average area of cavitation cloud projection) for UH with a diameter of 4.8 mm at different horn amplitudes (20 %, 30 %, and 40 %), different ambient pressures (100 kPa, 200 kPa, and 300 kPa) within DW, FW, SW, and SAT. The average cavitation size increases with increasing horn amplitude at all ambient pressures and in all solutions. Comparing the average cavitation cloud in the different solutions, we can again observe the aforementioned increase in average cavitation size between DW, FW, and SW, peaking in SW and then decreasing in SAT. Since vapor pressure decreases and both viscosity and surface tension increase with increasing salinity, one might expect a different behaviour. However, these differences are very small in FW and SW compared to DW (see Table S1). To further examine this behaviour, the salinity was finely swept between 0 and 360 ‰. In this case, the experiments were performed with 3 mm tip diameter, at 100 kPa and 40 % amplitude setting only. The results are presented in Fig. S3 in Supplementary Material. One can notice a similar behaviour of average cavitation cloud growth with increasing salinity up to some point (90 ‰ in this case). When salinity is further increased, a steep rise in cavitation cloud size is observed. After that, the cavitation cloud size decreases with increasing salinity and reaches a size similar to the one in DW at saturated solution. One possible explanation could be the coalescence inhibition mentioned earlier. The higher number of small cavitation nuclei probably facilitates the formation and growth of the cavitation cloud. After their collapse and fragmentation, the bubbles may remain small and numerous, which likely promotes the development of the cloud in the next cycle. The transition concentration for NaCl is about 0.1 M or about 6 g per kg of water (6 ‰ salinity) [14,15], but can be significantly increased when the approach speed of the bubbles is high (order of 100 mm/s) [16,17], which is likely to happen under UH. This could be the reason for a steep rise in cavitation cloud size between 90 and 120 ‰ salinity (Fig. S3). Once coalescence inhibition is established, further increase in salt concentration shows no additional effect on coalescence [14]. However, the viscosity increases, and the vapor pressure decreases with increasing salinity (Table S1). A combination of these two effects is likely to prevail at high salt concentrations (above 120 ‰) and the cavitation cloud is gradually suppressed. Nevertheless, further investigation is needed to fully understand this behaviour.

The right part of Fig. 5 shows the comparison of the characteristic cloud oscillation frequency between different ambient pressures, UH

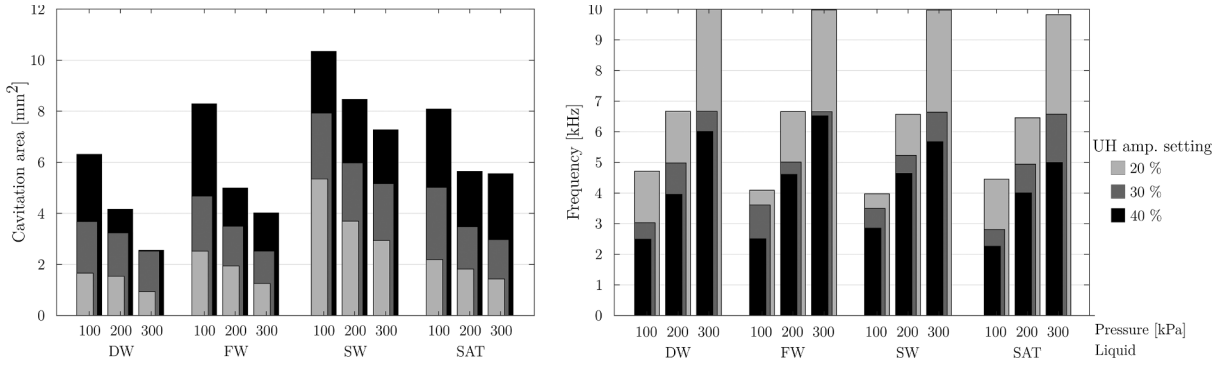

Fig. 5. Left: Cavitation cloud size comparison between various ambient pressures (100 kPa, 200 kPa, and 300 kPa), UH amplitudes (20 %, 30 %, and 40 %) and within different solutions (DW, FW, SW, and SAT). Right: Characteristic cavitation cloud oscillation frequency comparison between various ambient pressures (100 kPa, 200 kPa, and 300 kPa), UH amplitudes (20 %, 30 %, and 40 %) and within different solutions (DW, FW, SW, and SAT). Results for UH tip diameter of 4.8 mm are present in all cases.

amplitude settings and within different solutions at UH tip with 4.8 mm diameter. It can be clearly seen that the frequency increases with ambient pressure for all UH amplitudes and all solutions studied. If we compare the frequencies between the different solutions, we can see rather small differences. At an ambient pressure of 300 kPa and the lowest horn amplitude (20 %), the characteristic frequency reaches the highest average value of 9950 Hz and deviates by less than 1.5 %. This characteristic frequency is a half of the driving frequency of the horn (20 kHz). At an ambient pressure of 200 kPa and an amplitude setting of 20 %, the typical frequencies are also very similar with an average value of 6600 Hz, which is one-third of the horn driving frequency. At an ambient pressure of 100 kPa, the characteristic frequency differs significantly between the solutions studied and is lowest at SW. The characteristic oscillation frequency of the cavitation cloud is strongly correlated with the average size of the cavitation cloud (Fig. 5 - left). However, the deviations of characteristic frequencies are pronounced at 40 % and 30 %, while they are less noticeable at 20 % amplitude setting. This is probably due to the inertia of the cavitation structures. The oscillations of smaller structures can easily be superimposed by the main frequency of the horn, in contrast to the bigger structures, which are less sensitive due to their higher inertia.

The frequency analysis of the background cavitation has also shown that not only the horn driving frequency and the main cavitation structure collapses influence its occurrence, but also a phenomenon with frequencies above the horn driving frequencies. The answer probably lies in the shock waves formed due to the collapse of the main cavitation structures. Fig. 6 shows that a single collapse of the main cavitation structure forms several shock waves whose occurrence frequency is above the driving frequency of the horn. This is in line with previous research by Johnston et al. [32], who reported that shock waves occur periodically and as a result of cavitation cloud collapse. For larger cavitation clouds the authors observed multiple shock fronts and contributed them to the non-uniform nature of the cloud collapse. Furthermore, recent research [33] shows that shock waves from collapsing bubbles occur with frequencies in the order of a few MHz, which is well above the fundamental driving frequency of 24 kHz and also in good agreement with here presented results. Here observed emitted shock waves passing through the liquid react with the individual vapour/gas structures away from the horn tip, causing them to oscillate, which resembles as flashing background.

3.3. Tip diameter dependency

The left part of Fig. 7 shows the comparison between two tip diameters, 3 mm and 4.8 mm, at different ambient pressures 100 kPa, 200 kPa, and 300 kPa and different amplitudes of UH. As expected, the average cavitation size increases with horn amplitude regardless of the horn tip diameter and as the ambient pressure increases, the average cloud size decreases. The cavitation cloud is also proportionally larger for a wider tip. However, this relationship is pressure and amplitude dependent. Although the ratio of the tip areas of the horns is constant, the ratios of cavitation cloud sizes of differently sized horns vary depending on UH operating conditions. This is due to the effect already discussed in *Sec*. 3.1 and Fig. 3 (for a 4.8 mm tip), which is more pronounced with the larger horn. A similar comparison between two tip diameters at different operating conditions is shown in the right diagram in Fig. 7, where the typical cavitation cloud size oscillation frequencies are shown. Again, it can be observed that the characteristic frequency decreases with increasing amplitude but increases with increasing ambient pressure. Comparing the effects of horn size, the trend is opposite to that in the left diagram in Fig. 7. The cavitation cloud under a wider tip has a lower oscillation frequency under the same operating conditions (same pressure and amplitude). This is a direct consequence of cloud size, since larger clouds require more time to collapse. At higher ambient pressures, the size difference between 3 and 4.8 mm becomes smaller for the same amplitude setting. This is closely related to the trend of decreasing cloud size difference explained in *Sec*. 3.1.

3.4. Immersion depth dependency

Fig. 8 shows how the immersion depth of UH affects the extent of cavitation in distilled water for a tip diameter of 3 mm at constant ambient pressure (100 kPa) and amplitude setting (40 %). The cavitation behaviour does not change with immersion depth, only when the distance between the tip and the free liquid surface is minimised - due to turbulence in the vicinity of the tip the air gets mixed with the liquid. The immersion depth was varied between 0.3 cm and 9 cm, with 0.3 cm being the limitation due to liquid–air mixing and 9 cm being the limitation due to the length of the horn tip. It can be clearly seen that the magnitude of cavitation does not change, while the UH power increases with immersion depth. As the immersion depth increases, the submerged area increases, resulting in more friction between the solid horn tip and the liquid. Since UH tends to keep the amplitude constant, the power must be increased.

3.5. Acoustic cavitation number and empirically found relations

In this section, we present the formulation of an acoustic cavitation parameter and its relation to the size of the cavitation cloud under the tip of an ultrasonic homogenizer. The parameter is based on the acoustic cavitation number proposed by Dular and Petkovšek [23]. They derived the parameter from the hydrodynamic cavitation number (Eq. (1)). Although the ambient pressure (p_∞), vapor pressure (p_v), and density of the liquid (ρ) are easily determined in both hydrodynamic and acoustic cavitation experiments, it is difficult to define and measure the equivalent velocity in the case of cavitation under an ultrasonic horn. Dular and Petkovšek used a combination of acoustic impedance and intensity to derive the maximum velocity of the horn and introduced it into the equation (Eq. (1)) to obtain the acoustic cavitation number:

$$\sigma = \frac{2(p_\infty - p_v(T_\infty))cA_d}{\pi^2 P}, \tag{2}$$

where p_∞ is the ambient pressure, p_v is the vapor pressure of the liquid at the ambient temperature T_∞, c is speed of sound in the examined liquid, P is the average power of ultrasonic homogenizer, and A_d is the area of the horn's tip, determined by (Eq. (3)):

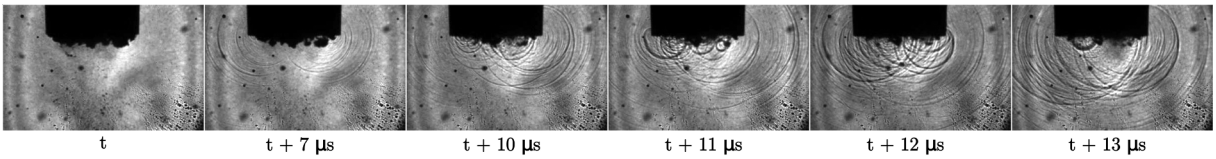

Fig. 6. Example of recording of shock waves, which were emitted at cavitation cloud collapse under an ultrasonic horn (d = 3 mm). Recorded by high-Speed Video Camera Shimadzu HPV-X2 at 2 Mfps. A femtosecond laser (EXPLA FemtoLux 3, 515 nm wavelength) was used for backlite illumination. Approximately 200 fs long laser pulses were synchronized with the image acquisition such that a single laser pulse illuminated each frame. This technique allowed us to avoid all motion blurring and imaging of the shock waves.

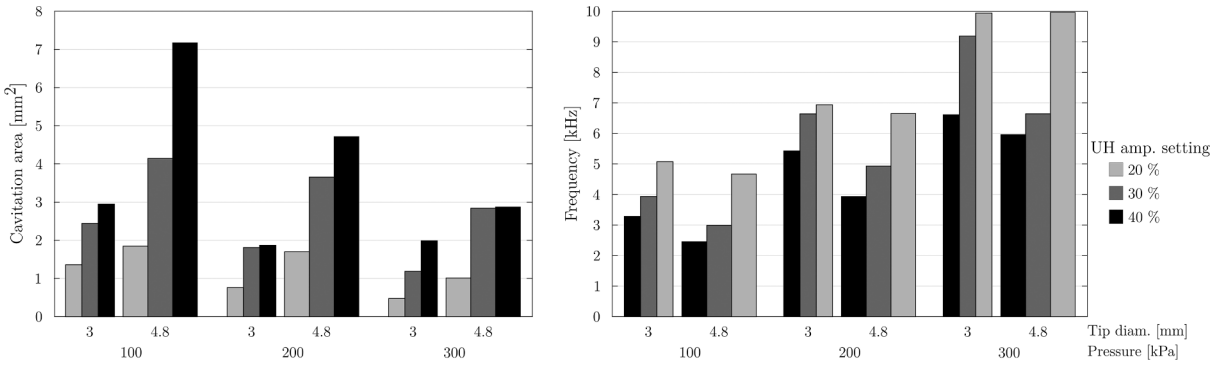

Fig. 7. Left: Cavitation cloud size comparison between two UH tip diameters (3 mm and 4.8 mm) in DW at different ambient pressures (100 kPa, 200 kPa, and 300 kPa) and horn amplitude settings (20 %, 30 %, and 40 %). Right: Characteristic cavitation cloud size oscillating frequency comparison between two UH tip diameters (3 mm and 4.8 mm) in DW at different ambient pressures (100 kPa, 200 kPa, and 300 kPa) and horn amplitude settings (20 %, 30 %, and 40 %).

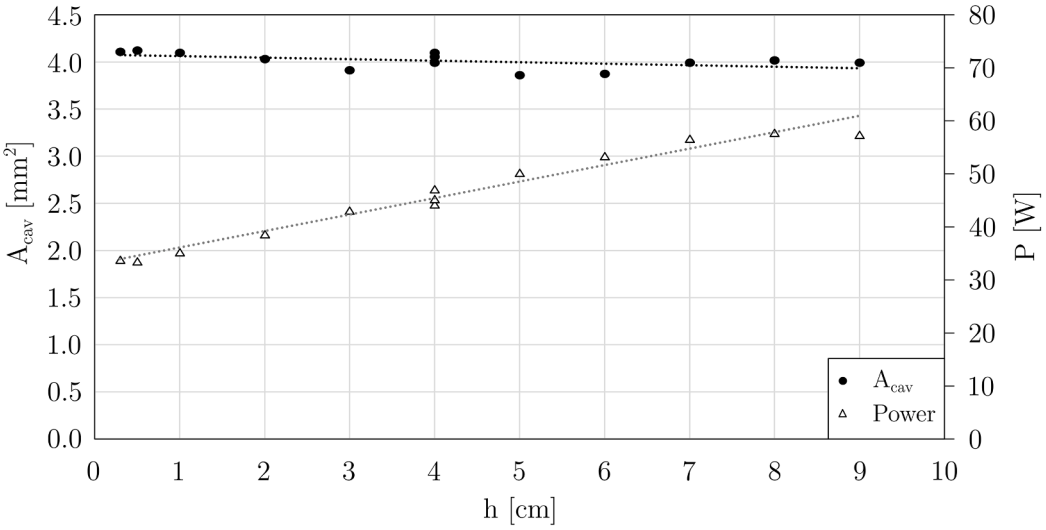

Fig. 8. Cavitation cloud size (black points) and UH power consumption (white triangles) dependency on UH tip immersion depth. Experiments were performed in distilled water, with 3 mm horn diameter, at 100 kPa ambient pressure and 40 % amplitude setting.

$$A_d = \pi \frac{d^2}{4}, \tag{3}$$

where d is the diameter of the horn. The proposed parameter includes both liquid properties (vapor pressure and speed of sound) and operating conditions (ambient pressure and power). The characteristics of the ultrasonic homogenizer are also included in the expression (area of the horn's tip). At the same time, these variables can be relatively easily determined either by measurements or literature.

Fig. 8 shows the relationship between the proposed acoustic cavitation number and the area of the cavitation cloud for two different sets of data. The white points show the measurements from UH with a horn diameter of 4.8 mm. This group includes experiments with three different amplitude settings (20 %, 30 %, 40 %), three ambient pressures (100, 200, and 300 kPa), and four different salt solutions (DW, FW, SW, SAT), giving a total of 36 points. The black points represent measurements made with the same device with 3 mm horn diameter at identical amplitudes, ambient pressures, and salt solutions. Additionally, results where salinity (green points), pressure (orange points) and immersion depth (blue points) were gradually varied are also included in the diagram.

One can observe a strong correlation ($R^2 > 0.82$ for both cases) between the cavitation number and the area of the cavitation cloud for each group of data. This indicates that the ambient pressure, liquid properties (vapor pressure and speed of sound), and average power consumption are well characterized by the proposed nondimensional parameter. However, there is a noticeable shift between groups differing only in horn diameter (white and black points) which indicates that the effect of horn size is inadequately represented by the proposed acoustic cavitation number. Furthermore, the results where the immersion depth was varied (blue points), form a horizontal line rather than following the trend. The immersion depth h is not part of the parameter σ but is indirectly included in the relationship through the UH power consumption P, which is immersion depth dependent (see Section 3.4).

To further examine the relationship between the cavitation cloud size and selected variables, a nonlinear regression analysis was used. A statistical model of the form:

$$A_{cav}(\Delta p, P, d, c, h) = K \Delta p^A P^B d^C c^D h^E, \tag{4}$$

where Δp is a pressure difference between the ambient pressure and the vapor pressure, P is the average power consumption, d is the horn's tip diameter, c is the speed of sound, h is the immersion depth and K is an arbitrary constant, was evaluated with all experimental results available (105 points in total). Optimal exponents (A-E), 95 % confidence intervals and respective statistical significance values (p – values) are summarized in Table 1.

One can notice a high significance (low p – values) of variables Δp, P

and d, with their optimal exponents close to unit. Calculated exponents of Δp and P are in accordance with those described in parameter σ. Cavitation cloud size (A_{cav}) is proportional to σ^{-1} (see Fig. 9), which indicates that A_{cav} is proportional to Δp^{-1} and P^1, similar to the results obtained by nonlinear regression. In contrast, the regression analysis demonstrates that A_{cav} is proportional to d^1, whereas the σ parameter suggested that A_{cav} is correlated with d^{-2} (Eq. (5)) and failed to predict the effect of horn tip diameter (Fig. 9).

$$A_{cav} \propto \sigma^{-1} = \frac{\pi^2 P}{2\Delta p c A_d} = \frac{2\pi P}{\Delta p c d^2} \tag{5}$$

Based on theoretical background of parameter σ and correlations obtained by regression analysis, we formulate a new parameter ψ (Eq. 6). The exponents of Δp and P are fixed to −1 and 1 due to their physical background (σ parameter) and a similar prediction by regression analysis. The exponent of d is corrected to −2, based on the regression model. The exponent of speed of sound (c) is kept −1, the same as in σ^{-1} expression (Eq. (5)), due to its theoretical background. One should notice that the 95 % confidence interval of the regression model (Table 1) also includes the −1 value for exponent of c. However, the confidence interval is broad and further studies are required to confirm the suggested relationship between cavitation cloud size and speed of sound. The immersion depth (h) is excluded from the ψ expression due to lack of theoretical background, limited experimental data (experiments were only performed in DW, at 100 kPa and 40 % amplitude) and poor correlation with cavitation cloud size.

$$\psi = K \frac{Pd}{\Delta p c} \quad [mm^3] \tag{6}$$

Fig. 10 presents the relationship between cavitation cloud size (A_{cav}) and new parameter ψ. Experimental results within different solutions (DW, FW, SW, SAT), with various tip diameters (3 and 4.8 mm), ambient pressures (100, 200 and 300 kPa) and amplitudes (20, 30 and 40 %) are presented. Experiments where pressure (75–300 kPa) and salinity (0–360 ‰) were finely swept are also included. The corresponding linear model is shown ($R^2 = 0.90$). One can observe that the linear model crosses the x-axis at some value ψ_0. This indicates that the cavitation cloud will be suppressed at a certain value of ψ, even before it reaches 0. The similarity to hydrodynamics, where such a value is called the cavitation inception number, is obvious. The × -intercept can be easily calculated from the constants K_1 and n_1 of the linear model equation (Fig. 10), giving a value of $\psi_o = 0.055$. However, the suppression of cavitation at low ψ numbers needs further investigation and empirical validation to accurately determine the $\psi_{inception}$ value.

4. Conclusions

The present study deals with acoustic cavitation induced by an ultrasonic horn, where cavitation dynamics was systematically investigated. The general objective of the research was to find the correlation between the operating conditions, liquid properties, and cavitation behaviour in order to describe the cavitation properties with a parameter that implies a basic representation of the cavitation size or volume under the horn tip.

In the scope of this study, the amplitudes of the ultrasonic horn, the geometry of the tip, the horn immersion depth, and the ambient pressure were varied in distilled water with different salt concentrations. The results show that the cavitation size is strongly dependent on the ambient pressure and the sonotrode amplitude setting. Higher ambient pressure and lower sonotrode amplitude decrease the cavitation size under the horn tip. Cavitation under the horn tip can be distinguished between the main cavitation region - the main cavitation adhering to the tip - and the cavitation scattered away from the cavitation cloud, described in the paper as the background cavitation, which consists of several individual cavitation bubbles or even larger cavitation structures. The frequency of collapse of the main cavitation cloud depends strongly on the size of the cavitation cloud, with a larger cavitation cloud taking more time to grow and collapse, resulting in lower frequencies. The background cavitation can oscillate at frequencies higher than the driving frequency of the horn because the shock waves generated by the collapse of the main cloud propagate its growth and collapse. A single collapse of the main cloud can produce multiple shock waves emanating from the different starting positions of the horn tip. The addition of salt, even in small amounts, significantly changes the size and appearance of the cavitation. Although low concentrations of salt have little effect on the surface tension, viscosity, and vapor pressure of the solution, the coalescence of the bubbles is inhibited, resulting in an increase in the size of the cavitation cloud. However, in highly

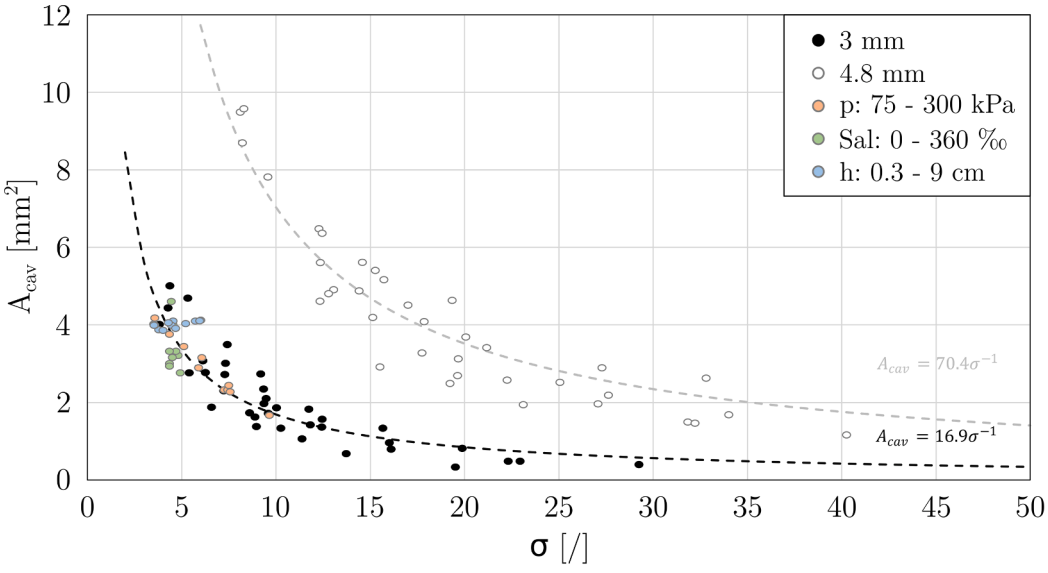

Fig. 9. Correlation between the area of the cavitation cloud and proposed acoustic cavitation number for 2 different UH configurations: i) UH with 3 mm tip (black, green, orange and blue points), ii) UH with 4.8 mm tip (white points). Experiments at different amplitude settings (20, 30 and 40 %), system pressures (100, 200 and 300 kPa) and salt solutions (DW, FW, SW and SAT) are included in both groups of data. Results where salinity (green), pressure (orange) and immersion depth (blue points) were finely swept are also included in the diagram. Dotted lines illustrate power law models with respective equations. (For interpretation of the references to colour in this figure legend, the reader is referred to the web version of this article.)

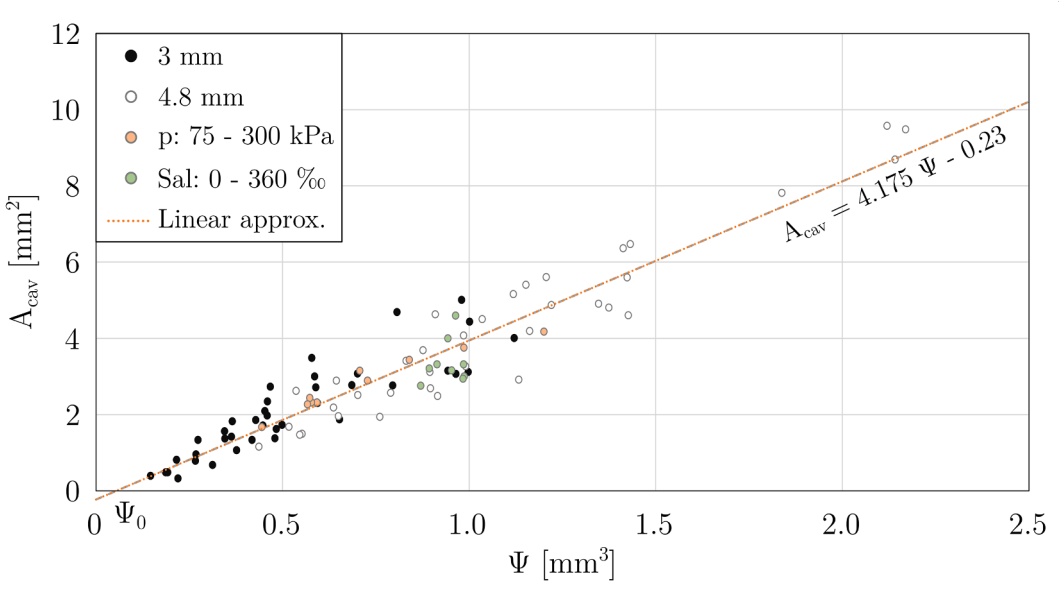

Fig. 10. Average cavitation cloud area plotted against the parameter ψ. Results with both 3 mm (black points) and 4.8 mm (white points) tips at different amplitude settings (20, 30 and 40 %), system pressures (100, 200 and 300 kPa), and salt solutions (DW, SW, FW and SAT) are shown. Results with fine variation of pressure (orange points) and salinity (green points) are also included. Corresponding linear model is represented by a dotted line and respective equation. (For interpretation of the references to colour in this figure legend, the reader is referred to the web version of this article.)

concentrated saline solutions, where the effects of viscosity and vapor pressure predominate, cavitation is attenuated.

Finally, the proposed acoustic cavitation number, derived from the classical hydrodynamic cavitation number, exhibits a strong correlation with the size of the cavitation cloud for data sets with the same tip diameters. Nonlinear regression analysis was used to correct the acoustic cavitation number and form a new cavitation parameter ψ that shows strong correlation with the area of the cavitation cloud for all experimental conditions studied, except immersion depth variation. Moreover, the cavitation cloud is apparently suppressed before the parameter ψ reaches 0. This suggests the existence of a ψ-value analogous to the cavitation inception number in hydrodynamics.

An attempt to characterise cavitation appearance and dynamics by a single parameter is an important step towards scaling-up of acoustically driven cavitation devices, which is a mayor bottleneck in the advancement of ultrasonic technology.

Author contributions

M.P. accepted the role of the leading author, he designed, developed, and partially performed experimental work, as well as partly analysed and evaluated visualization data. G.K. and J.Z. performed experimental work, analysed and evaluated visualization data. M.H. and M.D. analysed and evaluated visualization data. All authors contributed to the writing of the manuscript. All authors have approved the final version of the manuscript.

Funding Sources

This research was funded by the Slovenian Research Agency (Programs No. P2-0401, P2-0422 and Projects No. J2-3044, J7-1814, BI-DE/20-21-011).

Declaration of Competing Interest

The authors declare that they have no known competing financial interests or personal relationships that could have appeared to influence the work reported in this paper.

Data availability

Data will be made available on request.

Acknowledgment

The authors acknowledge the financial support from the Slovenian Research Agency (Programs No. P2-0401, P2-0422 and Projects No. J2-3044, J7-1814, BI-DE/20-21-011).

Appendix A. Supplementary data

Supplementary data to this article can be found online at https://doi.org/10.1016/j.ultsonch.2022.106159.

References

[1] W.T. Richards, A.L. Loomis, The chemical effects of high frequency sound waves I. A preliminary survey, J. Am. Chem. Soc. 49 (1927) 3086–3100, https://doi.org/10.1021/ja01411a015.
[2] L. Zhou, J. Zhang, L. Xing, W. Zhang, Applications and effects of ultrasound assisted emulsification in the production of food emulsions: A review, Trends Food Sci. Technol. 110 (2021) 493–512, https://doi.org/10.1016/j.tifs.2021.02.008.
[3] T.S. Perdih, M. Zupanc, M. Dular, Revision of the mechanisms behind oil-water (O/W) emulsion preparation by ultrasound and cavitation, Ultrason. Sonochem. 51 (2019) 298–304, https://doi.org/10.1016/j.ultsonch.2018.10.003.
[4] B.A. Bhanvase, D.V. Pinjari, P.R. Gogate, S.H. Sonawane, A.B. Pandit, Process intensification of encapsulation of functionalized CaCO3 nanoparticles using ultrasound assisted emulsion polymerization, Chem. Eng. Process. Process Intensif. 50 (2011) 1160–1168. https://doi.org/https://doi.org/10.1016/j.cep.2011.09.002.
[5] M. Petkovšek, M. Dular, Cavitation dynamics in water at elevated temperatures and in liquid nitrogen at an ultrasonic horn tip, Ultrason. Sonochem. 58 (2019) 104652, https://doi.org/10.1016/J.ULTSONCH.2019.104652.
[6] I. Tzanakis, M. Khavari, M. Titze, D.G. Eskin, Cavitation in thermoplastic melts: New insights into ultrasound-assisted fibre-impregnation, Compos. Part B Eng. 229 (2022) 109480, https://doi.org/10.1016/J.COMPOSITESB.2021.109480.
[7] Y. Fang, T. Yamamoto, S. Komarov, Cavitation and acoustic streaming generated by different sonotrode tips, Ultrason. Sonochem. 48 (2018) 79–87. https://doi.org/https://doi.org/10.1016/j.ultsonch.2018.05.011.
[8] W. Lauterborn, T. Kurz, Physics of bubble oscillations, Reports Prog. Phys. 73 (10) (2010) 106501, https://doi.org/10.1088/0034-4885/73/10/106501.
[9] A. Moussatov, C. Granger, B. Dubus, Cone-like bubble formation in ultrasonic cavitation field, Ultrason. Sonochem. 10 (2003) 191–195, https://doi.org/10.1016/S1350-4177(02)00152-9.

[10] A. Žnidarčič, R. Mettin, C. Cairós, M. Dular, Attached cavitation at a small diameter ultrasonic horn tip, Phys. Fluids 26 (2) (2014) 023304.
[11] J.-P. Franc, J.-M. Michel, Fundamentals of Cavitation, Kluwer Academic Publishers, 2004 https://doi.org/10.1017/CBO9781107415324.004.
[12] I. Tzanakis, G.S.B. Lebon, D.G. Eskin, K.A. Pericleous, Characterizing the cavitation development and acoustic spectrum in various liquids, Ultrason. Sonochem. 34 (2017) 651–662, https://doi.org/10.1016/j.ultsonch.2016.06.034.
[13] M. Firouzi, T. Howes, A.V. Nguyen, A quantitative review of the transition salt concentration for inhibiting bubble coalescence, Adv. Colloid Interface Sci. 222 (2015) 305–318, https://doi.org/10.1016/j.cis.2014.07.005.
[14] J. Zahradník, M. Fialová, V. Linek, The effect of surface-active additives on bubble coalescence in aqueous media, Chem. Eng. Sci. 54 (1999) 4757–4766, https://doi.org/10.1016/S0009-2509(99)00192-X.
[15] C.L. Henry, C.N. Dalton, L. Scruton, V.S.J. Craig, Ion-specific coalescence of bubbles in mixed electrolyte solutions, J. Phys. Chem. C 111 (2007) 1015–1023, https://doi.org/10.1021/jp066400b.
[16] V.V. Yaminsky, S. Ohnishi, E.A. Vogler, R.G. Horn, Stability of aqueous films between bubbles. Part 1. The effect of speed on bubble coalescence in purified water and simple electrolyte solutions, Langmuir 26 (2010) 8061–8074, https://doi.org/10.1021/la904481d.
[17] L.A. Del Castillo, S. Ohnishi, R.G. Horn, Inhibition of bubble coalescence: Effects of salt concentration and speed of approach, J. Colloid Interface Sci. 356 (2011) 316–324, https://doi.org/10.1016/j.jcis.2010.12.057.
[18] C.P. Ribeiro, D. Mewes, The effect of electrolytes on the critical velocity for bubble coalescence, Chem. Eng. J. 126 (1) (2007) 23–33, https://doi.org/10.1016/J.CEJ.2006.08.029.
[19] K.A. Rybkin, Y.K. Bratukhin, T.P. Lyubimova, O. Fatallov, L.O. Filippov, Experimental study of formation and dynamics of cavitation bubbles and acoustic flows in NaCl, KCl water solutions, J. Phys. Conf. Ser. 879 (2017), https://doi.org/10.1088/1742-6596/879/1/012026.
[20] B. Niemczewski, Maximisation of cavitation intensity in ultrasonic cleaning in aqueous solutions through selection of salt solution, Trans. IMF. 89 (2011) 104–108, https://doi.org/10.1179/174591911X12956245649027.
[21] D. Sunartio, M. Ashokkumar, F. Grieser, Study of the coalescence of acoustic bubbles as a function of frequency, power, and water-soluble additives, J. Am. Chem. Soc. 129 (2007) 6031–6036, https://doi.org/10.1021/ja068980w.
[22] M. Ashokkumar, R. Hall, P. Mulvaney, F. Grieser, Sonoluminescence from aqueous alcohol and surfactant solutions, J. Phys. Chem. B 101 (1997) 10845–10850, https://doi.org/10.1021/jp972477b.
[23] M. Dular, M. Petkovšek, Cavitation erosion in liquid nitrogen, Wear. 400–401 (2018) 111–118, https://doi.org/10.1016/j.wear.2018.01.003.
[24] A. Šarc, T. Stepišnik-Perdih, M. Petkovšek, M. Dular, The issue of cavitation number value in studies of water treatment by hydrodynamic cavitation, Ultrason. Sonochem. 34 (2017) 51–59, https://doi.org/10.1016/j.ultsonch.2016.05.020.
[25] A.P. Keller, Cavitation scale effects - Empirically found relations and the correlation of cavitation number and hydrodynamic coefficients. CAV 2001 Fourth Int. Symp. Cavitation, 2001. https://caltechconf.library.caltech.edu/92/.
[26] A. Žnidarčič, R. Mettin, M. Dular, Modeling cavitation in a rapidly changing pressure field – Application to a small ultrasonic horn, Ultrason. Sonochem. 22 (2015) 482–492, https://doi.org/10.1016/J.ULTSONCH.2014.05.011.
[27] L. Yusuf, M.D. Symes, P. Prentice, Characterising the cavitation activity generated by an ultrasonic horn at varying tip-vibration amplitudes, Ultrason. Sonochem. 70 (2021), 105273, https://doi.org/10.1016/J.ULTSONCH.2020.105273.
[28] S.N. Katekhaye, P.R. Gogate, Intensification of cavitational activity in sonochemical reactors using different additives: Efficacy assessment using a model reaction, Chem. Eng. Process. Process Intensif. 50 (2011) 95–103, https://doi.org/10.1016/J.CEP.2010.12.002.
[29] K. Turcheniuk, C. Trecazzi, C. Deeleepojananan, V.N. Mochalin, Salt-assisted ultrasonic deaggregation of nanodiamond, ACS Appl. Mater. Interfaces 8 (2016) 25461–25468, https://doi.org/10.1021/ACSAMI.6B08311.
[30] R. Pflieger, S.I. Nikitenko, M. Ashokkumar, Effect of NaCl salt on sonochemistry and sonoluminescence in aqueous solutions, Ultrason. Sonochem. 59 (2019) 104753, https://doi.org/10.1016/J.ULTSONCH.2019.104753.
[31] T.O. Oolman, H.W. Blanch, Bubble coalescence in stagnant liquids, Chem. Eng. Commun. 43 (1986) 237–261, https://doi.org/10.1080/00986448608911334.
[32] K. Johnston, C. Tapia-Siles, B. Gerold, M. Postema, S. Cochran, A. Cuschieri, P. Prentice, Periodic shock-emission from acoustically driven cavitation clouds: A source of the subharmonic signal, Ultrasonics 54 (2014) 2151–2158, https://doi.org/10.1016/J.ULTRAS.2014.06.011.
[33] M. Khavari, A. Priyadarshi, A. Hurrell, K. Pericleous, D. Eskin, I. Tzanakis, Characterization of shock waves in power ultrasound, J. Fluid Mech. 915 (2021) 3, https://doi.org/10.1017/JFM.2021.186.